

# Gaussian decomposition of H I surveys

## V. Search for very cold clouds

U. Haud

Tartu Observatory, 61 602 Tõravere, Tartumaa, Estonia  
e-mail: urmas@aai.ee

Received January 23, 2010; accepted January 23, 2010

### ABSTRACT

**Context.** In the previous papers of this series, we have decomposed into Gaussian components all the H I 21-cm line profiles of the Leiden-Argentina-Bonn (LAB) database, and studied statistical distributions of the obtained Gaussians.

**Aims.** Now we are interested in separation from the general database of the components the “clouds” of closely spaced similar Gaussians. In this paper we examine the most complicated case for our new cloud-finding algorithm – the clouds of very narrow Gaussians.

**Methods.** To separate the clouds of similar Gaussians, we start with the single-link hierarchical clustering procedure in five-dimensional (longitude, latitude, velocity, Gaussian width and height) space, but make some modifications to accommodate it to the large number of components. We also use the requirement that each cloud may be represented at any observed sky position by only one Gaussian and take into account the similarity of global properties of the merging clouds.

**Results.** We demonstrate that the proposed algorithm enables us to find the features in gas distribution, which are described by similar Gaussians. As a test, we apply the algorithm for finding the clouds of the narrowest H I 21-cm line components. Using the full sky search for cold clouds, we easily detect the coldest known H I clouds and demonstrate that actually they are a part of a long narrow ribbon of cold clouds. We model these clouds as a part of a planar gas ring, deduce their spatial placement, and discuss their relation to supernova shells in the solar neighborhood. Many other narrow lined H I structures are also found.

**Conclusions.** We conclude that the proposed algorithm satisfactorily solves the posed task. In testing the algorithm, we found a long ribbon of very cold H I clouds and demonstrated that all the observed properties of this band of clouds are very well described by the planar ring model. We also guess that the study of the narrowest H I 21-cm line components may be a useful tool for finding the structure of neutral gas in solar neighborhood.

**Key words.** ISM: atoms – ISM: clouds – Radio lines: ISM

### 1. Introduction

In earlier papers of this series, we described the Gaussian decomposition of large H I 21-cm line surveys (Haud 2000, hereafter Paper I) and the usage of the obtained Gaussians for the detection of different observational and reductional problems (Haud & Kalberla 2006, hereafter Paper II), for the separation of thermal phases in the interstellar medium (ISM; Haud & Kalberla 2007, hereafter Paper III) and for the studies of intermediate and high velocity hydrogen clouds (IVCs and HVCs; Haud 2008, hereafter Paper IV). A detailed justification for the use of Gaussian decomposition in such studies was provided in Paper III. Observational data for the decomposition were from the LAB database of H I 21 cm line profiles, which combines the new revision (LDS2, Kalberla et al. 2005) of the Leiden/Dwingeloo Survey (LDS, Hartmann 1994) and a similar Southern sky survey (IARS, Bajaja et al. 2005) completed at the Instituto Argentino de Radioastronomía. The LAB database is described in detail by Kalberla et al. (2005). Our method of Gaussian decomposition generated 1 064 808 Gaussians for 138 830 profiles from LDS2 and 444 573 Gaussians for 50 980 profiles from IARS.

In Papers II-IV, we used every obtained Gaussian as a single entity, which is independent of all other Gaussians, and analyzed statistical distributions of their parameters. The obtained results indicated that different structures in the ISM could be recognized

as density enhancements in the distribution of Gaussian parameters in the five-dimensional parameter space, or that the well defined Gaussians with similar parameters at least statistically define in the real space the related objects, which share the same physical state. The situation may be more complicated in the cases of heavily blended Gaussians in emission lines near the Galactic Plane. These earlier papers demonstrated also the importance of the Gaussian widths, the knowledge of which helps us separate the components, corresponding to different physical structures of the ISM or to the artifacts of the observations, reduction and the Gaussian decomposition itself. The third point, clear from the earlier studies, is that in reality many H I structures, observable in sky, extend to much larger areas than that covered by a single beam of the radio telescope. This means that some Gaussians of the neighboring profiles may represent the features of a similar origin, they are not independent of the others, and may be grouped together to represent larger structures.

In the present paper, we start studying these similarities and relations between the Gaussians – we define clouds of similar Gaussians, which may (but need not) describe the real gas concentrations in the real space. In doing so, we must keep in mind that there are no precise definitions of the terms such as “cloud”, “clump”, or “core” (Larson 2003), and the physical reality of the clumps, found by different authors, has been a matter of controversial debates since the presentation of the first systematic attempts to identify any kind of gas clumps. Nevertheless, many

papers are devoted to the study of clouds, clumps and cores in the ISM.

As the structure in molecular clouds determines, in part, the locations, numbers, and masses of newly formed stars, specifically great effort has been invested in characterizing the structure of this gas. Such statistical analysis of the molecular line data has usually followed one of two paths (Rosolowsky et al. 2008). Either authors construct statistical descriptions of the emission from an entire molecular line data set, or segment the data into what they believe to be physically relevant structures, and study the distribution of properties in the resulting population of objects.

Common examples of statistical analysis include fractal analysis (Elmegreen & Falgarone 1996; Stutzki et al. 1998),  $\Delta$ -variance (Stutzki et al. 1998; Bensch et al. 2001), correlation functions (Houllahan & Scalo 1990; Rosolowsky et al. 1999; Lazarian & Pogosyan 2000) and principle component analysis (Heyer & Brunt 2004). Statistical analysis produces many interesting comparisons between and among data, but physical interpretation of the statistics can be complicated. The segmentation and identification techniques are favored in the cases where the emission is thought to be comprised of physically important substructures (Rosolowsky et al. 2008).

The clumpy substructure of molecular clouds was first identified by eye (Blitz & Stark 1986; Carr 1987; Loren 1989; Nozawa et al. 1991; Lada et al. 1991; Blitz 1993; Dobashi et al. 1996). However, as a power law mass spectrum predicts an increasing number of smaller and smaller clumps, confusion is usually the limiting factor in clump identification by eye. It is thus highly desirable to use automated clump finding algorithms in the analysis of observed data, as the use of an algorithm allows to analyze the structure in a consistent and stable way (Kramer et al. 1998).

The two applications of the segmentation approach that have most shaped molecular line astronomy are the clump identification algorithms GAUSSCLUMP by Stutzki & Güsten (1990) and CLUMPFIND by Williams et al. (1994). GAUSSCLUMPS uses a least square fitting procedure to decompose the emission iteratively into one or more Gaussian clumps. CLUMPFIND associates each local emission peak and the neighboring pixels with one clump (similar to the usual eye inspection procedure). Although the basic concept of both algorithms is quite different, they give consistent results for the larger clumps, when used on the same data (Williams et al. 1994). In the lower mass range, the emission is assigned to additional smaller clumps in the Gaussian decomposition algorithm, and to the irregular extensions of the more massive clumps by CLUMPFIND. In both cases, an implicit assumption is made that the radial velocity coordinate can be replaced by the radial distance, but this assumption is not necessarily always satisfied (Ostriker et al. 2001).

With H I data Thilker (1998) has used an algorithm, somewhat similar to GAUSSCLUMPS, which creates a predefined set of various possible clouds, and applied it to look for H I bubbles blown by supernovas in external galaxies. The method, similar to CLUMPFIND, was used by de Heij et al. 2002 to automatically search for compact high velocity clouds (HVCs) in the Leiden/Dwingeloo Survey. However, instead of scanning for clouds along contours of constant intensity at varying levels, they used the gradient of the intensity field to determine the structure to which the pixels should be assigned.

Later Nidever et al. (2008) have used the Gaussian decomposition of the LAB profiles with the algorithm created according to the description of our decomposition program in Paper I. The obtained Gaussians are then used to disentangle over-

lapping H I structures. They stress that by using Gaussians, it is possible to distinguish different H I filaments even when they are overlapping in velocity. They state that in these situations the Gaussians trace structures that are real, and they may even hold physical information about the structures. They were successful in tracking tenuous structures through rather complicated environments even though the decomposition of those environments likely holds no physical meaning. The results were used to study the origin of the Magellanic Stream and its leading arm.

In this paper, we would like to move a step further and present an automatic computer program for finding different continuous H I features in the full decomposition of the LAB database. In the next section, we describe our algorithm for finding coherent structures in the large database of Gaussians, and in the following section, we apply this algorithm to look for the coldest H I clouds in the Galaxy, which could be identified using the LAB data. This search has been used for testing the new program as we may expect the clouds of very narrow Gaussians to be the hardest to find for our algorithm. However, when doing the search, we must keep in mind that the widths of such narrow Gaussians most likely are not correct representations of the actual widths of the underlying H I 21-cm emission lines. Due to both the finite optical depth of the lines and the velocity resolution of the LAB survey, the Gaussian widths used in this paper are only the upper limits for the actual line widths. Therefore, they cannot be used for the study of physical properties in the found clouds, but as the actual lines are even narrower than the corresponding Gaussians, we may still state that we are looking for very narrow lines and very cold gas clouds.

## 2. The cloud finding algorithm

### 2.1. The problems

The task of finding the clouds of similar objects belongs to cluster analysis. As in previous papers of this series we have studied some distributions of Gaussians, considering all components more or less independent of each other, it is now natural to follow some agglomerative (bottom-up) hierarchical clustering procedure. If we are looking for clouds, whose parameters vary smoothly from one point to another, the most appropriate algorithm seems to be single-link clustering: we add to the existing cluster a new element, which is the closest to at least one of the elements of this cluster.

To find the closest pairs, we need to know the distances between all Gaussians in 5-dimensional space (two sky coordinates and three Gaussian parameters for every component). However, here we face three problems. First of all, what is the distance between two Gaussians? After answering this, we may compute the distances, but need to store the results somewhere for the future use. As mentioned in the Introduction, we have 1 509 381 Gaussians and consequently 1 139 114 746 890 distances between them. If we want to store all these and for every distance also the identifications of the Gaussians, between which it is calculated, we need a storage of about 12.4 TBytes. Today this is clearly possible, but by no means reasonable.

When the first two problems are more or less mathematical, the third one is physical. In the Galaxy, H I has a rather complicated spatial and kinematic structure, and therefore the Gaussian decompositions of the profiles, particularly near the galactic plane, may be rather complicated and contain many different Gaussians per one profile. Running the preliminary versions of our cluster identification program demonstrated that without applying special restrictions, one dominating cloud started

to emerge around the galactic plane from the first steps of the merging process and finally only these H I structures were distinguishable, whose properties very strongly differ from those of general ISM. We would like to achieve rather opposite results: to separate all the pieces of more or less coherent structures and follow them as close as possible to other structures, but not to merge probably different features. Therefore, the simplest version of the single-link clustering is not acceptable, and we have to modify the clustering process somehow to better suit our interests.

## 2.2. Similarity of Gaussians

An important step in any cluster finding process is the selection of a distance measure, which will determine how the similarity of two elements is calculated. In our case, this problem may be divided into two subproblems: one is the distance of the observed profiles on the sky and another the comparison of the shapes of the Gaussians. The first subproblem has a standard solution – according to spherical trigonometry, the distance,  $e$ , between two observing directions with galactic coordinates  $(l_1, b_1)$  and  $(l_2, b_2)$  is given by

$$\cos e = \sin b_1 \sin b_2 + \cos b_1 \cos b_2 \cos(l_1 - l_2). \quad (1)$$

Concerning the second subproblem, different measures may be applied. After testing some possibilities, we decided to quantify the dissimilarity of two Gaussians  $E_i$  and  $E_j$  with the parameter

$$S' = \frac{\int_{-\infty}^{\infty} (E_i - E_j)^2 dV}{\int_{-\infty}^{\infty} E_i^2 dV + \int_{-\infty}^{\infty} E_j^2 dV}, \quad (2)$$

where the Gaussians  $E$  are given by

$$E(x) = T \exp \left[ -\frac{(x - V)^2}{2W^2} \right], \quad (3)$$

$T$  is the height of the component at its central velocity  $V$ , and  $W$  determines the width of the Gaussian.  $S'$  characterizes the squares of the deviations of one Gaussian from another, normalized by the sum of the squares of the deviations of both components from the zero line. If two Gaussians are exactly the same  $S' = 0$ , and when they become more and more different  $S' \rightarrow 1$ .

After integration we may write

$$S' = 1 - 2 \frac{T_i W_i T_j W_j}{T_i^2 W_i + T_j^2 W_j} \left( \frac{2}{W_i^2 + W_j^2} \right)^{1/2} \exp \left[ -\frac{(V_i - V_j)^2}{2(W_i^2 + W_j^2)} \right]. \quad (4)$$

We can see that computationally this formula is somewhat inconvenient as in the most interesting region of near zero values,  $S'$  is found as a difference of two nearly equal quantities, which is very sensitive to roundoff errors. At the same time, the exact meaning of the distance parameter, used in computations, is actually unimportant as long as it is any monotonic function of a parameter, which has a meaningful interpretation. Therefore, for computations we may replace the parameter  $S'$  with  $S = -\ln(1 - S')$ , and we get

$$S = \frac{(V_i - V_j)^2}{2(W_i^2 + W_j^2)} - \ln \left[ 2 \frac{T_i W_i T_j W_j}{T_i^2 W_i + T_j^2 W_j} \left( \frac{2}{W_i^2 + W_j^2} \right)^{1/2} \right]. \quad (5)$$

The parameter  $S$ , as defined by Eq. 5, compares the values of two Gaussian functions at all possible velocities and corresponds well to the natural human understanding of the similarity

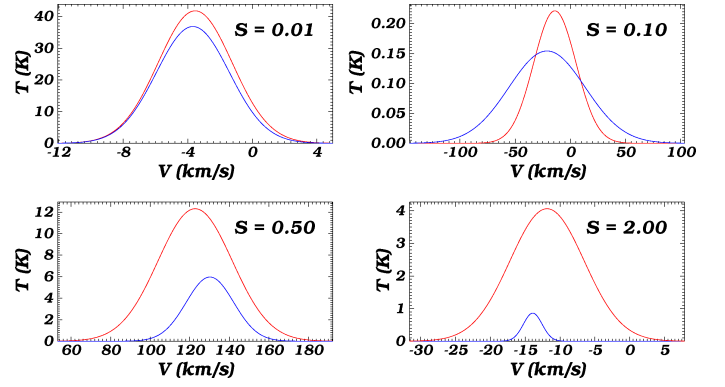


**Fig. 1.** Examples of pairs of Gaussians with different dissimilarity values  $S$ .

of two curves: the curves are similar when they are everywhere close to each other.  $S = 0$ , when two Gaussians have exactly the same values of their parameters and for increasingly different components  $S \rightarrow \infty$ . In Fig. 1 this is illustrated by some pairs of Gaussians with different values of  $S$ .

It is easy to see that this definition also well compensates for uncertainties in the determination of the Gaussian parameters, as discussed in Sec. 4.2. of the Paper I. For example, in the presence of noise our decomposition program gives the most unreliable values for the central velocities and widths for the widest Gaussians (component D in Fig. 10 of Paper I). However, when the line widths become larger, the differences in central velocities and also in widths become less important in the first addend of Eq. 5. Therefore, we may conclude that our dissimilarity measure treats the observed lines of different width with more or less the same precision. This is good for comparison of two independent Gaussians, but may pose problems for the clustering, as all natural gradients in parameter values become increasingly important for narrower components. It may turn the detection of small, bright, but cold clouds of H I rather problematic. We will return to this in the next section of the paper, where we present the search results of the coldest clouds in the Galaxy.

## 2.3. Decreasing the storage needs

In the previous subsection, we divided the calculation of the “distance” between Gaussians into two different estimates (Eqs. 1 and 5). For general hierarchical clustering we must join the obtained estimates into one, but in our case this is not so important. The original LDS2 and IARS data are given in a regular grid and we are looking for continuous clouds. The cloud can be continuous only if it is observed at least in one neighboring profile of any given observation belonging to this cloud. However, in the regular grid we know in advance, which observations are the neighbors of the initial one. This knowledge considerably reduces the amount of required computations and the storage needs: there is no necessity to compute the distance of a given Gaussian from all others, but only from the components of the neighboring profiles and as the neighbors are on the sky at more or less equal distances, we may, at least in some approximation, ignore in the computation the spatial part of the Gaussian distances. With this simplification, the task is reduced to a manageable size, and most of the following decisions in the fine-tuning of the clustering algorithm were based on the comparison of the results of trial computations with existing cloud catalogs (mostly HVCs).

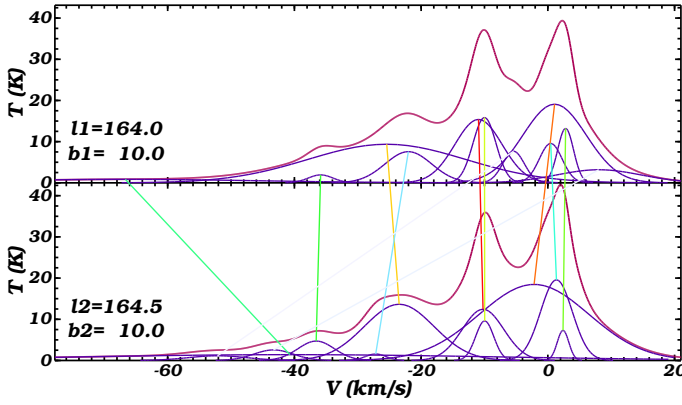


**Fig. 2.** Example of the pairing of Gaussians of two neighboring profiles. The Gaussian representations of the profiles are given with the raspberry lines and the individual Gaussian components with the violet ones. The colored straight lines connect the tips of the paired Gaussians. The hues of these lines (from red to blue) are given in the order of the goodness of the pair (from the best to the worst) and the saturations (HSV) are calculated as  $2.0/(2.0 + S)$ . Two nearly invisible alice blue and magnolia lines from the lower left to the upper right parts of the figure connect the clearly unrelated Gaussians. The connections correspond to  $S = 24.0$  and  $S = 44.8$ , and these pairs are not used in the clustering process. The centers of very wide components are sometimes located at rather different velocities, but they still may participate in the clustering process (spring green line from the lower center to the upper left, corresponding to  $S = 0.541$ ). A similar value of  $S$  for much narrower Gaussians is represented by a nearly vertical lime green line at about  $V = -36 \text{ km s}^{-1}$ .

The next step in further reduction of the storage needs was connected with the third problem, described at the beginning of this section: the avoidance of merging most Gaussians into one giant cloud around the galactic plane. We decided that every Gaussian of each profile represents a different feature in the real gas cloud. For example, in HVCs we often get two Gaussians in the same profile at nearly the same velocity, and most likely they both describe the same physical cloud, but the narrow Gaussian represents the properties of the gas in compact cold cores and the wider component describes the gas in the more extended warmer envelope of the cloud (Kalberla & Haud 2006; Paper IV). We decided to consider such features as different entities of ISM and therefore to apply a restriction that every cloud of Gaussians may contain only one component from each profile. In this way, if in some problems we need to consider “cores” and “envelopes” together, we may join corresponding clouds for this particular task, but if we allow them to merge from the beginning, it would be harder to separate different subclouds for some other studies.

This decision has a useful side-effect, that every Gaussian in one profile may have only one partner in each neighboring profile, and we need not store the distances between all possible combinations of the components of two neighboring profiles, but just one distance per every Gaussian in the profile with the smaller number of components. In other words, part of the global clustering process may be carried out locally between each pair of profiles by choosing in these profiles the best (most similar) pairs of Gaussians, and only the distances in these best pairs must be forwarded to the global merging phase of the algorithm. Such pairing of Gaussians of two neighboring profiles is illustrated in Fig. 2).

However, even forwarding of the distances of the best pairs may be restricted somewhat more. Not every Gaussian in one profile can be successfully paired with some other in a neighboring profile. Some features may be present only in a single profile, or do not propagate into other profiles in some particular direction. Of course, mathematically it is possible to find a partner for every Gaussian of the profile, which has less components in a pair of profiles, but for some such pairs of Gaussians the value of  $S$  becomes very large (in Fig. 2 the lines with the least saturated colors) and these large distances are clearly useless in the final clustering process. As a result, we stored the info only for those pairs, which had  $S < 2$ . Altogether we got in this way 4 946 775 distances or links between Gaussians.

## 2.4. The clustering algorithm

The final procedure for defining clouds was as follows:

1. find for profile at any  $(l, b)$  the  $(l \pm 0.5/\cos b, b)$ ,  $(l, b \pm 0.5)$  and  $(l \pm 0.5/\cos b, b \pm 0.5)$  partners;
2. for each pair of profiles calculate the dissimilarities (Eq. 5) of all possible pairs of Gaussians;
3. find the most similar pairs of Gaussians for each pair of profiles and store the links with  $S < 2$ ;
4. build the index of links in the ascending order of  $S$ ;
5. merge the pairs of Gaussians into clouds in the order of the found index.

At every merging step the following procedures were passed:

1. if two merging Gaussians already belonged to the same cloud, the corresponding link was rejected;
2. if two merging clouds contained different Gaussians from the same profile, the clouds were not merged and the corresponding link was rejected;
3. if the global properties of two merging clouds were too different, their merging was postponed;
4. all remaining links were stored into the list of active links (links, which have passed all the tests and therefore actually merge something).

The last but one procedure certainly needs some clarification. By using a pure single link clustering algorithm, we sometimes found the cases where two clouds with rather different average properties merged, as they touched each other at some point on their outer perimeter. As this was undesirable, we added a corresponding test and modified the algorithm somewhat in the direction of the global link methods. For this, when the merging of clouds, containing more than one Gaussian, was initiated by Gaussians with dissimilarity  $S$ , we:

1. calculated for both merging clouds their total emission profiles as a sum of all Gaussians in a particular cloud;
2. calculated the dissimilarity  $S_{Cl}$  for these profiles. Of course, now we had to do the integration in Eq. 3 numerically, and then apply the transform to get the result similar to  $S$  from Eq. 5 for single Gaussians;
3. made the decision about merging the clouds:
  - if  $S_{Cl} \leq S$ , corresponding clouds were merged and link  $S$  was written to the list of active links;
  - if  $S < S_{Cl} < 2$ ,
    - (a) the clouds were not merged,
    - (b) the value of  $S$  was replaced with  $S_{Cl}$ ,
    - (c) the original link was deleted from the ordered list of links,

- (d) a new link was generated in the list of links in the place, corresponding to the value of  $S_{Cl}$ ,
- (e) when some time later the clustering process reached that new link, it was treated as all other links between single Gaussians;
- if  $S_{Cl} \geq 2$ , the clouds were not merged and the corresponding link was rejected.

It may seem that the added procedure is rather limiting and determines the whole clustering process, but the actual tests did not confirm this. With merging the Gaussians, the widths of the resulting cloud profiles initially grow rapidly and the comparison of such wide profiles gives rather small values of  $S_{Cl}$ . As a result, at the beginning of the merging process the comparison of global properties of the merging clouds rarely changes the run of clustering. It becomes more important at later stages when the Gaussians with larger mutual differences are initiating the merging. Therefore, the outcome of the clustering process has not changed dramatically, but nevertheless the results are brought into better accordance with those, obtained from human inspection of the data.

As a result of the described algorithm, we obtained a list of 1 350 655 active links between Gaussians. It represents the clustering dendrogram and for getting a list of clouds or clusters, we must cut this dendrogram at an appropriate level.

### 3. Very cold clouds

#### 3.1. Finding the clouds

In the previous section, we discussed that the proposed cloud compilation algorithm is expected to work better with relatively wide Gaussians, but there may be certain problems with finding the coldest clouds of very narrow Gaussians. First tests in the width range, corresponding to HVCs, have shown that the results are acceptable, but we will return to this in our next papers. Here we would like to present the results for the worst case of very cold clouds.

To our knowledge, the coldest clouds in the Galaxy, found so far primarily in H I emission, are the two gas concentrations at near-zero velocity around ( $l = 225^\circ, b = +44^\circ$ ) and ( $l = 236^\circ, b = +45^\circ$ ), discovered by Verschuur (1969), and afterwards studied in more details by Verschuur & Knapp (1971) and Knapp & Verschuur (1972). Later the third cloud around ( $l = 213^\circ, b = +41^\circ$ ) was added to the first two by Heils & Troland (2003), and one of the recent detailed studies of these clouds is that by Meyer et al. (2006). They observed the interstellar Na I D1 and D2 absorption toward 33 stars, derived a cloud temperature of  $20^{+6}_{-8}$  K and placed a firm upper limit of 45 pc on the distance of the clouds. This distance corresponds to the upper limit of the linear size of the clouds of about 5 pc. Redfield & Linisky (2008) have interpreted these clouds as a result of the collision of warm high-velocity Gem Cloud with the slower moving Leo, Aur, and LIC Clouds in the Local Interstellar Medium (LISM). At the same time, the properties of the clouds seem to be also rather similar to the temperatures (mostly  $10 < T_S < 40$  K) and dimensions (in parsec scale) of numerous H I self-absorption features, found near the galactic plane (e.g. Gibson et al. 2000; Dickey et al. 2003; Kavars 2005; Hosokawa & Inutsuka 2007). Our interest in the subject is to test if the clustering algorithm finds these clouds and in the case of a positive answer, to look for similar features all over the sky.

For this test we first constructed the dendrogram for all Gaussians in our decomposition and inspected the resulting

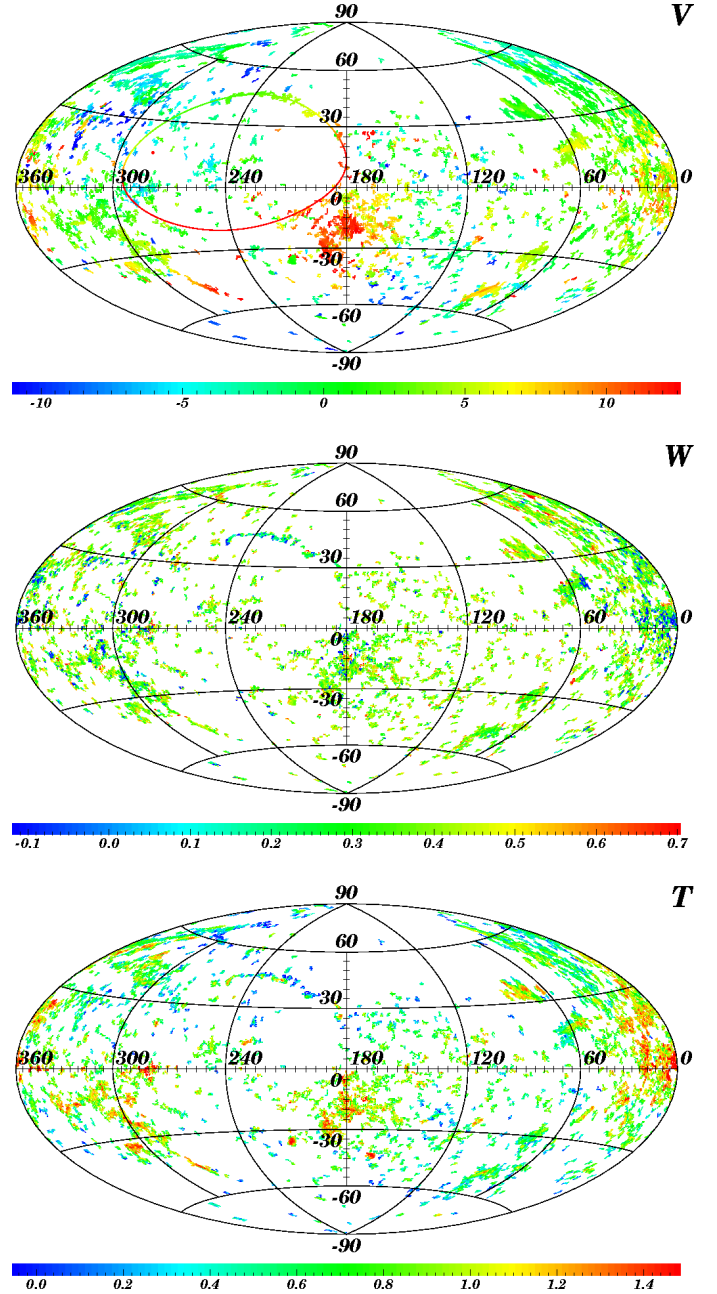


**Fig. 3.** The velocities, line-widths and brightness temperatures in clouds of at least 7 Gaussians, compiled by our clustering algorithm. Shown are the objects for which the mean Gaussian height is  $\geq 1.0$  K,  $FWHM \leq 3.0$  km s $^{-1}$ ,  $|V| \leq 15$  km s $^{-1}$  and the parameters of at least half of the Gaussians satisfy Eq. 4 of Paper II (components are likely not radio interferences). The color scales are for  $V$ ,  $\lg W$  and  $\lg T$ , respectively. The color line in the upper panel represents the sky positions and the velocities of our model ring (see Sec. 3.2).

clouds for different values of the cutting level of the dendrogram. From this inspection we chose for the final cutting level the value  $S_{Cu} = 0.44$ . In this way we obtained 94 874 clusters of Gaussians and 236 306 components remained detached from the others. The largest cloud (12 585 Gaussians) in the obtained list corresponds to relatively smooth warm neutral medium at high galactic latitudes, but the list contains also many very small clouds of 2-3 Gaussians in each (the cluster size distribution fol-

lows the power law with the slope of about 1.9). As Verschuur & Knapp (1971) have estimated that their cool clouds have diameters of at least  $1'.5$ , we are not interested in the smallest clouds in our list, and in the following, we will consider only the clouds, containing at least 7 Gaussians (in LAB one profile represents an area of 0.25 square degrees and 7 profiles cover the area, corresponding to the cloud with the diameter of  $1'.5$ ). In our list, there are 21 224 clouds of such size.

To search for the coldest clouds in the list, we must apply some additional selection criteria. First of all, we are looking for clouds, consisting of relatively narrow Gaussians. In Paper III, we demonstrated that the mean line-width of the H I 21-cm radio lines of the cold neutral medium of our Galaxy is  $FWHM = 3.9 \pm 0.6 \text{ km s}^{-1}$ . Therefore, the gas, having  $FWHM \leq 3.0 \text{ km s}^{-1}$ , may be considered already as a very cold gas and we will look for the clouds for which the mean width of the Gaussians is below this limit. In Paper II, we also demonstrated that many weak and/or very narrow Gaussians do not represent the actual H I emission of the Galaxy, but are more likely due to observational noise or radio interferences. Here we are not interested in these Gaussians, and therefore we apply the selection criteria, given by Eqs. 4 and 5 of Paper II. However, now we do not apply these criteria to single Gaussians, but to the clouds obtained from our clustering process.

From Eqs. 4 and 5 of Paper II, it follows that the narrowest Gaussians, which most likely represent the galactic H I, have the heights  $\geq 0.95 \text{ K}$ . Therefore, we consider only these clouds, for which the mean height of their Gaussians is  $\geq 1.0 \text{ K}$ . At first sight, a similar selection ( $FWHM \geq 1.25 \text{ km s}^{-1}$ , corresponding to Eq. 4 of Paper II) may also be applied to the width of the Gaussians. However, we are looking for clouds with the narrowest Gaussians, and some of the real lines may be even narrower than interferences with  $T \geq 1.0 \text{ K}$ . Therefore, as such selection may reject not only the interferences, but also a considerable amount of Gaussians of main interest in our study, this selection cannot be applied directly. At the same time, the selection rule given by Eq. 4 of Paper II, applies only statistically and it turned out that better results can be obtained by rejecting the clouds, for which more than half of their Gaussians do not satisfy Eq. 4 of Paper II. Nevertheless, some confusion with the interferences still remains.

After applying all the described selection criteria we received a list of 1380 cold clouds. However, when looking at these clouds we saw that the clouds with the highest velocities (concentrated around  $+50$  and  $+100 \text{ km s}^{-1}$ ) were located only in a very narrow band around the galactic plane (all at  $|b| < 22^\circ$ , most at  $|b| < 5^\circ$ ). We have stressed several times that in these regions the Gaussian decomposition gives relatively unreliable results, and the corresponding Gaussians are with high probability not directly related to the physical properties of the ISM. Therefore, we decided to reject also these clouds by applying the requirement  $|V| \leq 15 \text{ km s}^{-1}$  on the mean velocities of the clouds. In this way, we rejected 44 more small clouds. All remaining clouds are presented in Fig. 3.

When applying the described selection criteria on clusters, obtained with different values of the cutting level,  $S_{\text{Cu}}$ , of the dendrogram, we found that for  $0 < S_{\text{Cu}} < 0.27$  the number of Gaussians in the selected clouds increases rapidly. For  $0.27 \geq S_{\text{Cu}} < 0.75$ , the pictures similar to Fig. 3 remain nearly unchanged with only a slight maximum in the number of Gaussians for  $S_{\text{Cu}} = 0.44$ . After  $S_{\text{Cu}} = 0.75$  the number of Gaussians starts to decrease as gradually wider and wider Gaussians are linked to the existing clouds and the average line-widths of clouds grow above our selection limit. For Fig. 3, we chose the value of

$S_{\text{Cu}}$ , which gave the highest number of Gaussians in the selected clouds.

### 3.2. Verschuur's clouds

From Fig. 3, we can see that the cold clouds around ( $l = 225^\circ, b = +44^\circ$ ), ( $l = 236^\circ, b = +45^\circ$ ) and ( $l = 213^\circ, b = +41^\circ$ ), mentioned at the beginning of the previous subsection, are clearly visible. Moreover, in this figure these clouds seem to be a part of a more extended narrow string of clouds, covering on the sky about  $80^\circ$  from ( $l \approx 181^\circ, b \approx +20^\circ$ ) to ( $l \approx 258^\circ, b \approx +47^\circ$ ). This is in good agreement with the remark by Heils & Troland (2003), who mentioned that other narrow H I 21-cm emission lines could be found in the extended region around the clouds, studied in their paper. Nevertheless, they limited their interest only to the longitude interval of  $200^\circ \leq l \leq 240^\circ$  and reported the broken ribbon of cold H I gas stretching over  $20^\circ$  across the constellation Leo.

In more details, these clouds are plotted in Fig. 4. To better separate them from other features in the same sky region, we have used here even more severe selection criteria ( $FWHM \leq 2.7 \text{ km s}^{-1}$ ,  $2.25 \leq V \leq 11.55 \text{ km s}^{-1}$ ), compared to those for Fig. 3. However, to increase the sensitivity and as the noise Gaussians are rather effectively removed from the data also by using only clouds of 7 or more Gaussians, we have dropped here the requirement  $T \geq 1.0 \text{ K}$ . Due to the changes in selection criteria, the considerations, similar to those used for selecting the dendrogram cutting level  $S_{\text{Cu}} = 0.44$  for Fig. 3, have lead in this case also to somewhat higher  $S_{\text{Cu}} = 0.53$ . As a result, we have obtained a chain of clouds, which seems to follow some arc, well populated in its higher galactic longitude half and more opened at lower longitudes.

We can see a clear velocity gradient along this ribbon of clouds with the average velocities of the clouds increasing by about  $9 \text{ km s}^{-1}$  per length of the arc. A similar, but a much weaker gradient holds also for the line-widths: the average  $FWHM$  of the clouds increases by  $1 \text{ km s}^{-1}$  from the higher galactic longitudes towards the lower longitudes. It also appears that the clouds tend to be brighter near their centers than in outer regions, which is an expected behavior for real gas clouds. In this way, while also the lower longitude part of the string of clouds is interrupted in some places by voids, the coherence of its characteristics strongly indicates that it is really the same physical feature. It remains questionable, whether the clouds at ( $l = 237^\circ, b = 24^\circ, V = 2.3 \text{ km s}^{-1}$ ) and ( $l = 184^\circ, b = 25^\circ, V = 4.5 \text{ km s}^{-1}$ ) also belong to the same structure as they deviate from the others considerably on the sky or in velocity. Therefore, we have not used them in the following discussion.

The smoothness of the observed structure was rather tempting for its modeling. As arced shapes often hint at circular structures, seen under some angle to their plane, we decided to model this string of clouds and their velocities as a partial gas ring somewhere in space, which may move relative the Local Standard of Rest (LSR) as a whole and also rotate around its center and expand away from this center. We found that such model very well describes both, the apparent location of the clouds on the sky and their observed velocities. According to the obtained model, the center of the ring is located in the direction ( $l = 236.2 \pm 0.9^\circ, b = -13.2 \pm 0.3^\circ$ ), its apparent major axis is inclined by  $4.7 \pm 0.9^\circ$  to the galactic plane and the angle between the ring plane and the line of sight to its center is  $14.5 \pm 0.3^\circ$ . The radius of the ring is seen under the angle of  $41.8 \pm 0.3^\circ$  along the apparent major axis of the observed structure. The ring as a whole moves with the velocity of  $21.0 \pm 0.5 \text{ km s}^{-1}$  in the

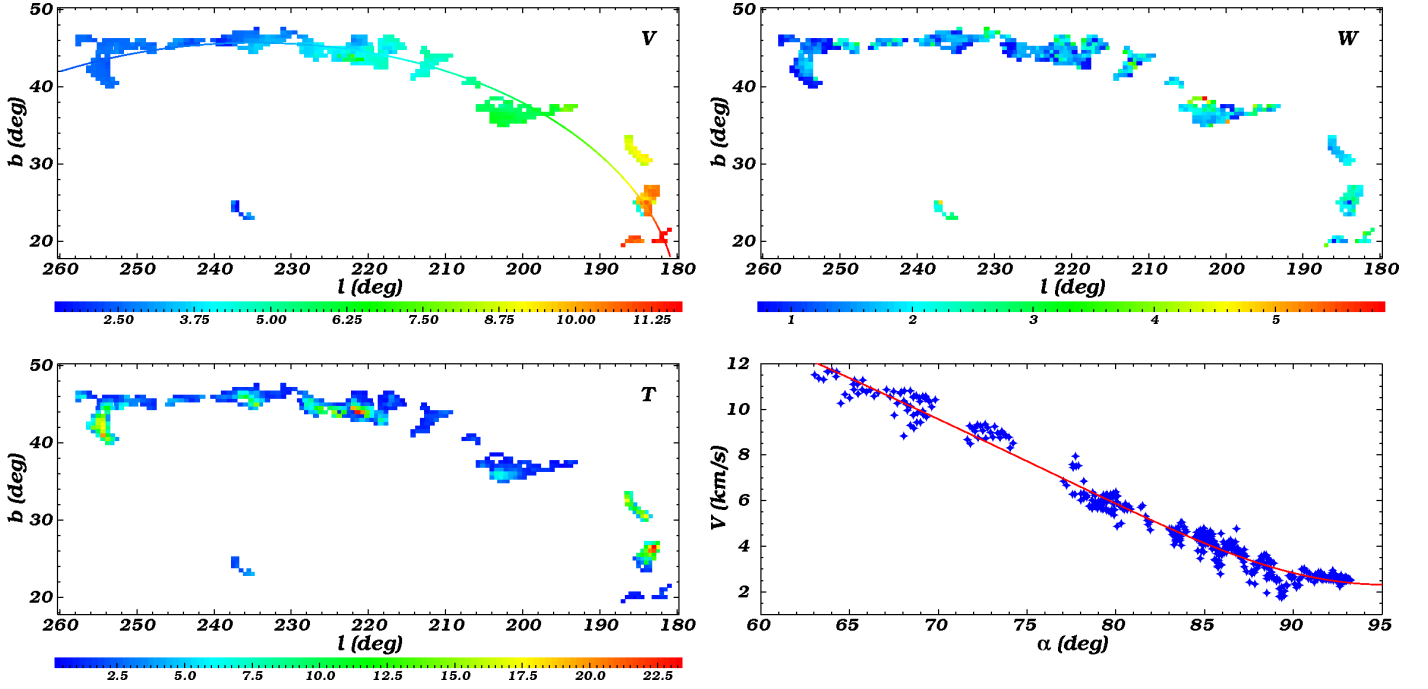


**Fig. 4.** The velocities, line-widths and brightness temperatures of the clouds in the region of the observable part of the ring. Shown are the objects, represented by at least 7 Gaussians, for which the mean Gaussian width  $FWHM \leq 2.7 \text{ km s}^{-1}$ ,  $2.25 \leq V \leq 11.55 \text{ km s}^{-1}$  and the parameters of at least half of the Gaussians satisfy Eq. 4 of Paper II (components are likely not radio interferences). The color scales are for linear values of  $V$ ,  $W$  and  $T$ . The color line in the upper left panel represents the sky positions and the velocities of our model ring. A more detailed comparison of the observed LSR velocities of the ring clouds (blue diamonds) with the model velocities (red line) is given in the lower right panel of the figure. Here the abscissa is a polar angle of the ring point in the ring plane.

direction ( $l = 193.3 \pm 1.2^\circ, b = 2.2 \pm 0.7^\circ$ ), rotates clockwise with the velocity of  $10.6 \pm 0.4 \text{ km s}^{-1}$  and its expansion speed is  $26.2 \pm 0.7 \text{ km s}^{-1}$ . As errors of these parameters are given the 99.73% confidence limits obtained from the bootstrapping.

The projection of the model ring onto the sky is shown with a line in the first (V) panels of Figs. 3 and 4. The color of the line corresponds to the line of sight velocity of each ring point. The fit of the model to the observed gas velocities is shown in the lower right part of Fig. 4. From Fig. 3, we can see that actually the same structure seems to continue even beyond the lower latitude border of Fig. 4, and it can be followed down to about ( $l = 225^\circ, b = -19^\circ$ ). However, this continuation of the ring is rather sparsely populated with relatively small clouds and is located near the galactic plane, where the Gaussian decomposition cannot be considered to be reliable. Therefore, we will not discuss this continuation in greater detail than just mentioning that when the parameters of the ring were estimated only from a  $30^\circ$  segment of the whole ring (as seen from the ring center and indicated in the lower right panel of Fig. 4), in total the visible part of the ring may extend to nearly half ( $162^\circ$ ) of the full circle. For the other half there seems to be no good candidates for the same structure. But, of course, also the location of the model ring is rather uncertain in these regions.

### 3.3. The ring in space

In most H I profiles the emission, corresponding to the clouds under discussion, appears as a very narrow and relatively strong line, not seriously blended by a broader-velocity, lower-intensity emission component. Therefore, it may seem to be easy to derive from the parameters of our Gaussians some estimates for

the physical conditions inside these clouds. Unfortunately, as briefly mentioned in the Introduction, this is not true. Already Verschuur & Knapp (1971) demonstrated that the shapes of these narrow emission lines are actually not Gaussians, but they are considerably influenced by saturation. They derived the spin temperature by assuming the optical depth to be a Gaussian function of the frequency and fitting the observational data to the equation of transfer. We cannot use even this path, as the velocity resolution of the LAB data is more than 10 times lower than that of the data used by Verschuur & Knapp (1971) and therefore the actual line-shapes are mostly unresolved.

Nevertheless, we decided to take a further step and to obtain at least some preliminary estimate for the distance of the ring. In doing so, we followed the procedure described by Haud (1990). These estimates are based on the assumption that a correlation exists in cold H I clouds between the clouds internal velocity dispersion and its linear dimensions, similar to the one observed for molecular clouds (Larson 1981 and many others since then). We will not discuss here all the questions, related to the existence or meaning of such correlation, but use it just as a possible tool, which may or may not give some acceptable results. We followed exactly the same procedure as described in Haud (1990) with the only exception that we did not correct the LSR velocities of the clouds to the Galactic Standard of Rest (GSR), as in this case it is most likely unjustified. Instead, we removed the large scale velocity gradients and projection effects in the ribbon clouds using our ring model. In this way, we obtained the distance estimates for all ring clouds and using our model of the ring, converted them to estimates of the distance of the ring center.

As expected, we got rather scattered results, but in general, the distance estimates of individual clouds agreed with our ring model, which indicates that the lower longitude tip of the band of clouds is located from us about twice as far as the higher longitude tip. As the scatter of the obtained estimates was considerably higher for estimates, based on smaller (covering fewer gridpoints of LDS observations) clouds than for those, based on larger clouds, we decided to accept for the distance of the ring center the weighted average of all determinations, and to use as weights the number of Gaussians in each cloud. In this way, we obtained a distance estimate of  $126 \pm 82$  pc. The error estimate corresponds only to the scatter of individual distance estimates and does not account for uncertainties in the ring model or in the method, used for obtaining these distances. To this distance corresponds the linear radius of the model ring of 113 pc and the distance of the Verschuur's cloud A of 34 pc, which is in good agreement with the upper distance limit (45 pc) for this cloud, established by Meyer et al. (2006).

Of course, with such a model a number of questions remain. First of all, why to model this structure as a planar ring of gas clouds, when most processes, which may give the expansion velocities, obtained for this ring, have more likely spherical symmetry? Moreover, when the ribbon of gas clouds covers nearly  $80^\circ$  in the galactic longitude, in our model this corresponds only to  $30^\circ$  along model ring itself. This means that actually we do not know anything about most of the ring, and therefore its parameters may contain large systematic errors. Also, the distance estimates are based on rather arbitrary assumptions, they are quite uncertain, and as the Gaussians most likely overestimate the widths of the actual underlying H I lines, they must be considered as upper limits for corresponding actual distances.

Nevertheless, even such model well demonstrates the coherence of the observed clouds, it seems to give some indication of possible continuation of the structure even beyond the region studied here, and it is interesting to see that the distance estimates of the individual clouds and the ring model are in general agreement with respect to the orientation of the gas band in 3-dimensional space. Moreover, we have seen that the observed behavior of the gas stream at lower longitudes may be understood in the framework of this model – in these regions the distance of the clouds from the Sun increases and therefore they become apparently smaller. As we have selected from our clustering results only relatively large clouds (at least 7 Gaussians in each cloud), we may lose most of these apparently smaller ones from our view. Therefore, beyond about ( $l = 182^\circ, b = 20^\circ$ ) and the distance 64 pc the stream becomes rather fragmentary and we can observe only some seemingly small clouds, which actually may have relatively large linear dimensions and line-widths. As here we cannot see any more the really smallest and coldest clouds, this may explain the increase of the average observable line-widths in this region. But why then the stream so abruptly terminates at its other end? This happens practically at the nearest point of the ring to the Sun.

Wolleben (2007) has proposed a model for the North Polar Spur (NPS) region. This model explains the results of the Dominion Radio Astrophysical Observatory Low-Resolution Polarization Survey (Wolleben et al. 2006), and the model consists of two synchrotron-emitting shells, S1 and S2 (Fig. 5). The same model shells were used by Frisch (2008) to explain the higher column densities of Ca II in the galactic quadrants  $l > 180^\circ$  versus  $l < 180^\circ$ . We studied the mutual placement of these shells and our ring, and found that the ring intersects with the shell S2 in the direction ( $l = 256^\circ, b = 43^\circ$ ) at the distance of 33 pc from the Sun. This position exactly matches the beginning

of our band of clouds, and the result is nearly independent of the rather indefinite determination of the linear size of the ring. Further to the higher longitudes the ring continues inside the S2 and probably the ring clouds are destroyed by the shell. The ring leaves the shell at ( $l = 295^\circ, b = 4^\circ$ ) at the distance of 85 pc from the Sun. As with the lower longitude end of the gas stream, we may expect that at these distances the ring clouds, even if they exist there, are mostly unobservable.

A problem with this explanation of the observability of the ring clouds is the fact that the ring intersects the S1 shell at ( $l = 235^\circ, b = 46^\circ, d = 33$  pc), but is still well observable to both sides of this point. Maybe only a slight disturbance of the velocities of the ring clouds can be seen in this region. However, the explanation of the different behavior of the ring clouds at the intersections with two different shells may lie in the different ages of these shells. According to Wolleben (2007), the S1 shell is about 6 million years old and observable only as a small part of “New-Loop” in the Southern galactic hemisphere. The S2 shell is 1-2 million years old and seems to be much more active as it is responsible for the well known NPS. Therefore, we may expect that the S1 shell is not any more energetic enough to destroy the ring clouds, as they are destroyed by S2. By arbitrarily using the standard model for the kinematic age of stellar wind bubbles (Weaver et al. 1977), we may estimate that the age of the ring itself is about 2.5 million years, quite comparable with the age of the S2 shell. However, the physical mechanisms responsible for the production of such cold clouds in the environment of the hot Local Bubble (LB) are still poorly understood (Stanimirović 2009).

### 3.4. Other cold clouds

In Fig. 3, we can also see some other concentrations of the gas besides the one described in previous subsections. Many of them are even more prominent than the narrow band of clouds, we have just discussed. Of those we can mention, for example, four clouds at approximately  $l = 70^\circ$  and  $b = -50^\circ, -30^\circ, 15^\circ, 35^\circ$ , but also the wide bands of clouds from ( $l = 10^\circ, b = 15^\circ$ ) to ( $l = 290^\circ, b = 70^\circ$ ), from ( $l = 30^\circ, b = 15^\circ$ ) to ( $l = 0^\circ, b = 70^\circ$ ) and from ( $l = 320^\circ, b = -10^\circ$ ) to ( $l = 260^\circ, b = -55^\circ$ ). Some very narrow Gaussians, seen in the IARS part of the LAB still represent radio interferences, and we will not discuss the concentrations near the galactic plane.

However, most of these gas concentrations differ from ring clouds in many respects. First of all, the average width of corresponding Gaussians is somewhat (up to 1.5 times) larger than that of the ring clouds. When in ring clouds the narrowest Gaussians form small knots in the environment of somewhat wider Gaussians, in many places of the concentrations, mentioned in this subsection, the situation seems to be quite opposite – small knots of wider Gaussians are surrounded by not so wide ones. The velocity distribution is also different. For the ring clouds, we may observe a very smooth velocity variation along the band of clouds and no velocity variations of the same magnitude inside individual clouds. For other gas concentrations, general velocity gradients are less prominent, but there are considerable velocity variations in the smaller regions. The only exception may be the cloud complex from ( $l = 320^\circ, b = -10^\circ$ ) to ( $l = 260^\circ, b = -55^\circ$ ), where the clouds further from the galactic plane have clearly higher velocities than those more close to the galactic plane.

The location of the ring clouds versus others on the sky is also considerably different. We demonstrated that the ring extends from the surface of S2 shell away towards the galactic an-

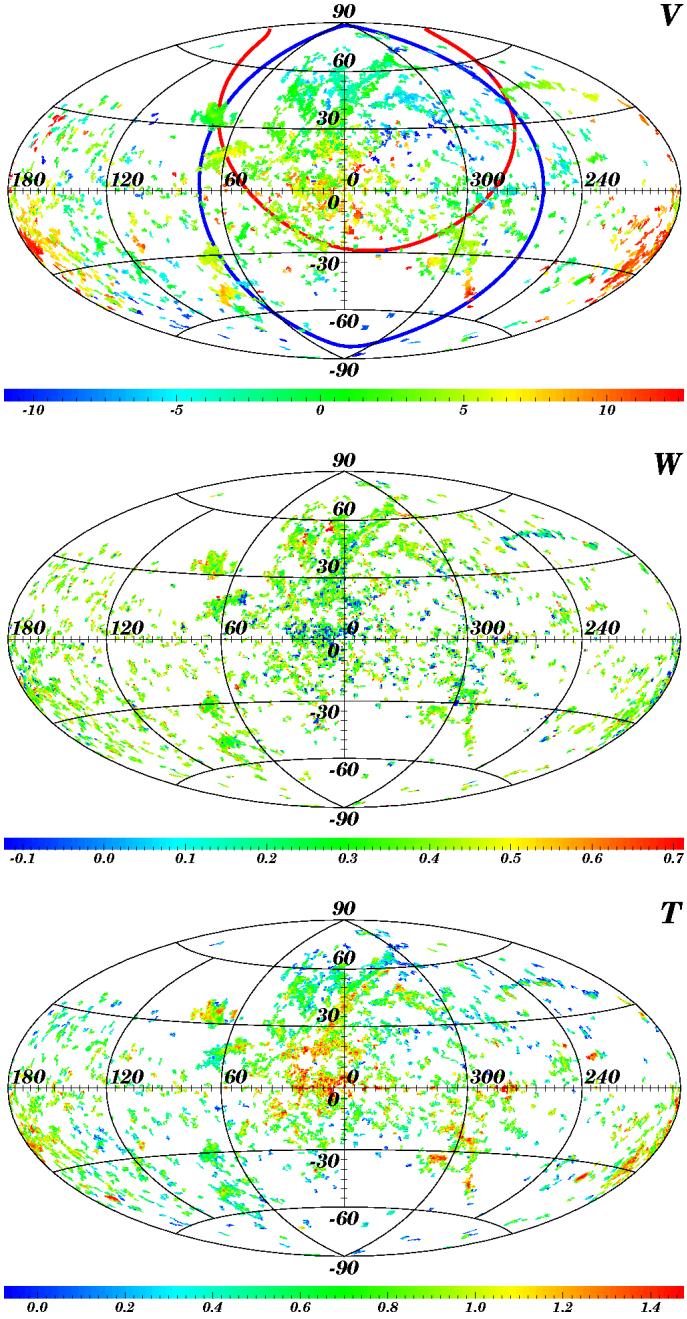


**Fig. 5.** The same as Fig. 3, but now centered on the galactic center and without the data about the ring model. Instead, the S1 and S2 shells are marked with thick background lines in the Vpanel. The red curve gives the visible outer boundary of the S2, but as we are located inside the S1, the blue curve only approximately outlines the region, containing the best visible part of S1.

ticenter region. We have not modeled the spatial locations of the other cloud complexes, but in projection onto the sky most of them seem more likely to follow the shapes of the best observable parts of the shells S1 and S2 than to intersect the surfaces of these shells (Fig. 5). The clouds from  $(l = 10^\circ, b = 15^\circ)$  to  $(l = 290^\circ, b = 70^\circ)$  and from  $(l = 30^\circ, b = 15^\circ)$  to  $(l = 0^\circ, b = 70^\circ)$  project onto the S2 shell and in their general shape seem to follow the regions, where the line of sight is tangent to shell S2, and therefore they may be related to the NPS.

The clouds at  $l = 70^\circ$  and  $b = -50^\circ, -30^\circ, 15^\circ, 35^\circ$  rather exactly border the best observable part of the S1 and may be

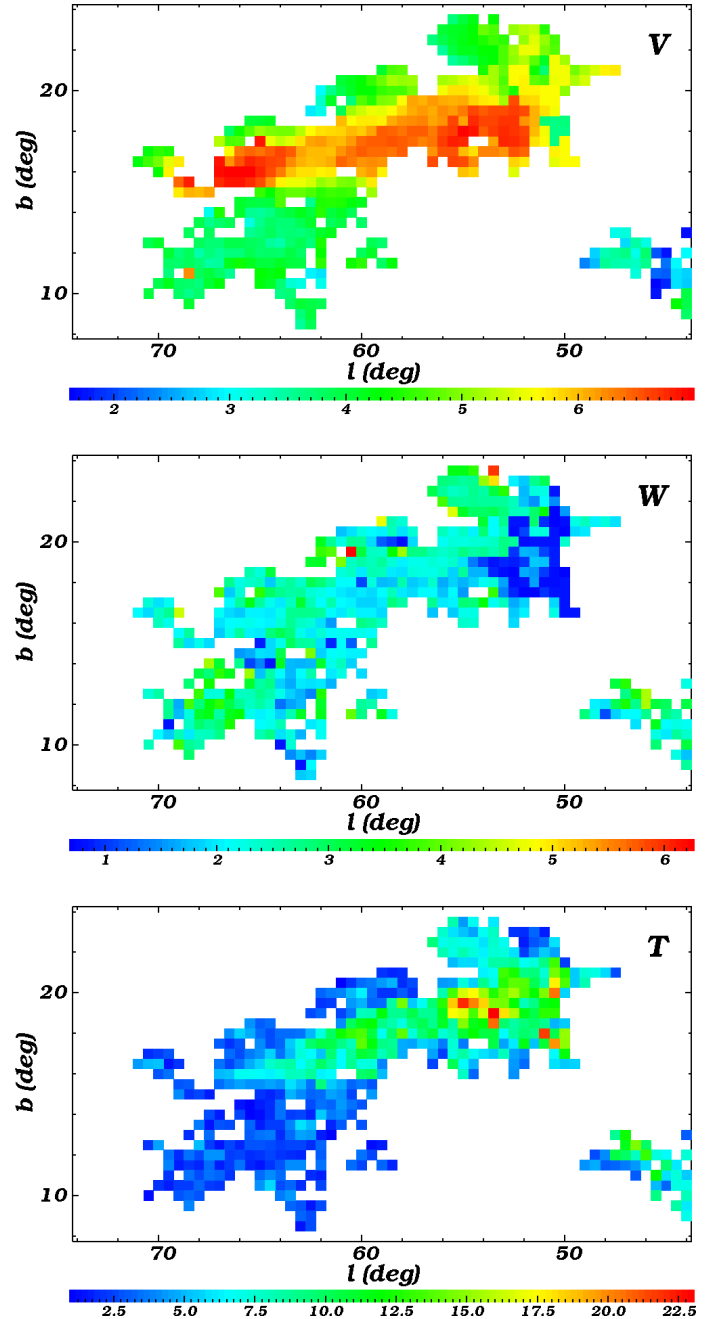


**Fig. 6.** The same as Fig. 4, but for clouds around  $l = 60^\circ, b = 15^\circ$  and without the data about the ring model.

therefore somehow related to this shell. Of these four clouds the one at about  $l = 60^\circ, b = 15^\circ$  extends in sky projection deepest into the shell S1 and maybe even into S2. It is interesting that also the internal structure of this cloud seems to hint at the interaction with external media (Fig. 6). Its densest parts have the highest velocities and resemble the stream of gas, nearly perpendicular to the borders of the images of the S1 and S2 shells. This relatively dense and fast-moving gas is mostly surrounded by the envelope with smaller observed line of sight velocities and surface densities. In front of the head of this comet-like stream (in the region, closest to the S1 and S2) is located the most narrow-lined (the coolest) gas. Other three clouds, which seem to be located further away from the shells surfaces, do not have such distinctive cometary structures. However, we must admit that also Fig. 6 changes, when we relax our selection criteria

on line widths. In this case, the stream obtains an extension with clouds of slightly wider lines in front of the "comet's" head. At the same time, as these additional clouds have smaller sizes and higher line widths, in space they may be located somewhere behind the "comet", illustrated in Fig. 6.

The gas from ( $l = 320^\circ, b = -10^\circ$ ) to ( $l = 260^\circ, b = -55^\circ$ ) once again seems to resemble the ring clouds. The stream projects onto the shell S1 and its location relative to S2 is very similar to that of the ring clouds: the stream starts near the outer boundary of the shell and extends nearly perpendicularly away from S2. Both the ring clouds and the stream described here have their smallest line of sight velocities near S2 and the velocities increase when moving away from the shell. At the same time, this Southern stream has much more un-ordered appearance than the ring clouds in the Northern sky. Nevertheless, there may be even a possibility to imagine that these Southern clouds form a part of our ring, but in this case the estimates for the ring parameters must be rather inaccurate. Actually, if this is the case, the real shape of the structure must considerably deviate from the perfect ring as it seems to be impossible to get an acceptable fit of the location and velocities of the Northern part of the ring when its Southern part is forced to follow the gas at ( $l = 320^\circ, b = -10^\circ$ ) to ( $l = 260^\circ, b = -55^\circ$ ).

#### 4. Conclusions

So far we have decomposed the LAB database of H I 21-cm line profiles into the Gaussian components (Paper I) and studied the statistical distributions of the obtained components (Papers II – IV). These distributions have revealed several interesting structures, but have given only the probabilities with which some particular Gaussian may belong to one or another structure. In this paper, we proposed an algorithm for grouping similar Gaussians. In this way, we free ourselves from the need to study each Gaussian separately, and we may expect that all the Gaussians of the "cloud" of similar components have the same nature. It may also be possible to obtain some additional physical information from the shapes and sizes of such clouds.

As a test problem, we have considered the separation of clouds of the narrowest Gaussians as on the basis of the preliminary considerations just this may be the hardest problem for our algorithm. We have demonstrated that actually the algorithm easily found the coldest known H I clouds discovered decades ago by Verschuur (1969). As expected, the tests indicated that, depending on the cutting level of the clustering dendrogram, our approach may divide some larger clouds into separate, most coherent substructures, but hopefully mostly avoids the merging of unrelated features. Such behavior was intentional, as it seems more appropriate to study a larger number of clouds of which everyone represents a certain type of line features than to have a smaller number of clouds which may mix Gaussians of different nature into one.

We also found that Verschuur's clouds form only a small part of a much longer ribbon of presumably very cold clouds covering on the sky about  $80^\circ$ . As the gas velocities and line widths vary along this ribbon rather smoothly, we decided to model the whole structure as a part of a planar gas ring which may move in space as a whole and also rotate around and expand away from its center. Such a model very well represented the observed properties of the gas stream and indicated that the ring center must be located at a distance of  $126 \pm 82$  pc from the Sun in the direction ( $l = 236^\circ.2 \pm 0^\circ.9, b = -13^\circ.2 \pm 0^\circ.3$ ). The ring radius is about 113 pc, its apparent major axis is inclined by  $4^\circ.7 \pm 0^\circ.9$  to the galactic plane and the angle between the ring

plane and the line of sight to its center is  $14^\circ.5 \pm 0^\circ.3$ . The ring as a whole moves with the velocity of  $21.0 \pm 0.5$  km s $^{-1}$  in the direction ( $l = 193^\circ.3 \pm 1^\circ.2, b = 2^\circ.2 \pm 0^\circ.7$ ), it rotates clockwise with the velocity of  $10.6 \pm 0.4$  km s $^{-1}$  and its expansion speed is  $26.2 \pm 0.7$  km s $^{-1}$ . In the framework of such model the apparent gradual weakening of the ring clouds at the lower longitude tip of the stream is explained by increasing distances between the Sun and the ring clouds in this region, and the abrupt end of the stream at the higher longitude part is caused by the intersection of the ring with the S2 supernova shell from the model by Wolleben (2007).

We have briefly discussed also other narrow-lined H I clouds, found by our clustering algorithm. In many respects most of them are somewhat different from the ring clouds (lines are slightly wider, velocities less coherent over the structures etc.). We have not attempted to model these features, but have noted that their locations on the sky may hint at their relation to supernova activities in the solar neighborhood. Anyway, as the line-widths of these clouds are also small, they must be relatively cold clouds and therefore not very large spatially. As these clouds of presumably small linear dimensions cover rather large areas on the sky, they probably cannot be located very far from the Sun and therefore the studies of such narrow-lined clouds may give useful information about the gas in the solar neighborhood. Usually this gas is studied through corresponding absorption lines, which allow estimation of physical conditions in the local gas. H I 21-cm emission line is less useful in this respect, but may be still usable for large scale surveys to find out possible interesting features in the local neighborhood.

As a result, we may state that the ring clouds seem to be a rather unique feature on the sky. Most likely they are the coldest clouds observable in the H I 21-cm emission line. Also slightly warmer clouds (clouds with slightly wider 21-cm emission lines) may be related to rather local gas structures inside or near the LB. There is some probability that also the gas from ( $l = 320^\circ, b = -10^\circ$ ) to ( $l = 260^\circ, b = -55^\circ$ ) may be related to the structure, which we called a ring, but in this case in larger scales the structure must considerably deviate from a perfect planar ring. Some properties of all these clouds may be similar to those of the H I self-absorption features, observed predominantly near the galactic plane, where our approach to the emission data is most likely not applicable, but in this paper we have not studied this in detail to make firm statements.

*Acknowledgements.* The author would like to thank W. B. Burton for providing the preliminary data from the LDS for program testing prior the publication of the survey. A considerable part of the work on creating the decomposition program was done during the stay of U. Haud at the Radioastronomical Institute of Bonn University (now Argelander-Institut für Astronomie). The hospitality of the staff members of the Institute is greatly appreciated. We thank drs. I. Kolka, E. Saar, P. Tenjes and K. Annuk for fruitful discussions. We also thank our anonymous referee whose suggestions have improved the clarity of the paper. The project was supported by the Estonian Science Foundation grant no. 7765.

#### References

- Bajaja, E., Arnal, E. M., Larrarte, J. J., et al. 2005, *A&A*, 440, 767
- Bensch, F., Stutzki, J., & Ossenkopf, V. 2001, *A&A*, 366, 636
- Blitz, L. 1993, *Giant Molecular Clouds*. In *Protostars and Planets III*, eds. E. H. Levy & J. I. Lunine (Tucson & London: The Univ. Arizona), 125 *ApJ*, 300, 89
- Blitz, L., & Stark, A. A. 1986, *ApJ*, 300, 89
- Carr, J. S. 1987, *A&A*, 323, 170
- de Heij, V., Braun, R., & Burton, W. B. 2002, *A&A*, 391, 159
- Dickey, J. M., McClure-Griffiths, N. M., Gaensler, B. M., & Green, A. J. 2003, *ApJ*, 585, 801
- Dobashi, K., Bernard, J. P., & Fukui, Y. 1996, *ApJ*, 466, 282
- Elmegreen, B. G., & Falgarone, E. 1996, *ApJ*, 471, 816

- Frisch, P.C. 2008, arXiv:0804.1901v1
- Gibson, S. J., Taylor, A. R., Higgs, L. A., & Dewdney, P. E. 2000, *ApJ*, 540, 851
- Hartmann, L. 1994, The Leiden/Dwingeloo Survey of Galactic Neutral Hydrogen, Ph. D.-Thesis, Leiden Univ.
- Haud, U. 1990, *A&A*, 230, 145
- Haud, U. 2000, *A&A*, 364, 83 (Paper I)
- Haud, U., & Kalberla, P. M. W. 2006, *Balt. Astron.*, 15, 413 (Paper II)
- Haud, U., & Kalberla, P. M. W. 2007, *A&A*, 466, 555 (Paper III)
- Haud, U. 2008, *A&A*, 483, 469 (Paper IV)
- Heils, C., & Troland, T. H. 2003, *ApJ*, 586, 1067
- Heyer, M. H., & Brunt, C. M. 2004, *ApJ*, 615, 45
- Hosokawa, T., & Inutsuka, S.-I. 2007, *ApJ*, 664, 363
- Houllahan, P., & Scalo, J. 1990, *ApJS*, 72, 133
- Kalberla, P. M. W., & Haud, U. 2006, *A&A*, 455, 481
- Kalberla, P. M. W., Burton, W. B., Hartmann, D., et al. 2005, *A&A*, 440, 775
- Kavars, D. W., Dickey, J. M., McClure-Griffiths, N. M., Gaensler, B. M., & Green, A. J. 2005, *ApJ*, 626, 887
- Knapp, G. R., & Verschuur, G. L. 1972, *AJ*, 77, 717
- Kramer, C., Stutzki, J., Rhring, R., & Corneliussen, U. 1998, *A&A*, 329, 249
- Lada, E. A., Bally, J., & Stark, A. A. 1991, *ApJ*, 368, 432
- Larson, R. B. 1981, *MNRAS*, 194, 809
- Larson, R. B. 2003, *Rep. Prog. Phys.*, 66, 1651
- Lazarian, A., & Pogosyan, D. 2000, *ApJ*, 537, 720
- Loren, R. B. 1989, *ApJ*, 338, 902
- Meyer, D. M., Lauroesch, J. T., Heils, C., Peek, J. E. G., & Engelhorn, K. 2006, *ApJ*, 650, 67
- Nidever, D. L., Majewski, S. R., & Burton, W. B. 2008, *ApJ*, 679, 432
- Nozawa, S., Mizuno, A., Teshima, Y., et al. 1991, *ApJS*, 77, 647
- Ostriker, E. C., Stone, J. M., & Gammie, C. F. 2001, *ApJ*, 546, 980
- Redfield, S., & Linsky, J. L. 2008, *ApJ*, 673, 283
- Rosolowsky, E. W., Goodman, A. A., Wilner, D. J., & Williams, J. P. 1999, *ApJ*, 524, 887
- Rosolowsky, E. W., Pineda, J. E., Kauffmann, J., & Goodman, A. A. 2008, *ApJ*, 679, 1338
- Stanimirović, S. 2009, *Space Sci. Rev.*, 143, 291
- Stutzki, J., & Güsten, R. 1990, *ApJ*, 356, 513
- Stutzki, J., Bensch, F., Heithausen, A., Ossenkopf, V., & Zielinsky, M. 1998, *A&A*, 336, 697
- Thilker, D. A., Braun, R., & Walterbos, R. A. M. 1998, *A&A*, 332, 429
- Verschuur, G. L. 1969, *ApL*, 4, 85
- Verschuur, G. L., & Knapp, G. R. 1971, *AJ*, 76, 403
- Weaver, R., McCray, J., Castor, J., Shapiro, P., & Moore, R. 1977, *ApJ*, 218, 377
- Williams, J. P., de Geus, E. J., & Blitz, L. 1994, *ApJ*, 428, 693
- Wolleben, M. 2007, *ApJ*, 664, 349
- Wolleben, M., Landecker, T. L., Reich, W., & Wielebinski, R. 2006, *A&A*, 448, 411